On-wafer Microstrip Meander-Line Slow-Wave Structure at Ka-band

Shaomeng Wang, *Member, IEEE*, Sheel Aditya, *Life Senior Member, IEEE*, Xin Xia, *Member, IEEE*, Zishan Ali, *Student Member, IEEE*, and Jianmin Miao, *Member, IEEE*

***Abstract*— A novel configuration for a Ka-band V-shaped microstrip meander-line slow-wave structure (SWS) is reported. The SWS is designed to work at a voltage less than 4 kV and provide a wide bandwidth. CPW input/output feed-lines and a shielding structure are incorporated to enable fast on-wafer cold test measurements on a CPW probe station without requiring dicing or a metal enclosure. Simulated dispersion characteristics and coupling impedance for the optimized design are presented. The simulated S11 of the entire structure is better than –15 dB over 25-36 GHz. The proposed configuration is fabricated using 4" Si wafers and standard microfabrication processes. The measured S11 of the entire structure is better than –10 dB over 20-40 GHz. The observed high insertion loss has been explained in detail and alternative approaches that can reduce the loss have been proposed. The PIC simulation results show that for a 3.6 kV, 50 mA sheet-beam the output power can potentially reach 14.5 W at 34 GHz with a gain of 21.6 dB. A 3 dB bandwidth of about 25% centered at 32 GHz is also indicated.**

***Index Terms*— Microstrip, meander line, slow wave structure, microfabrication, TWT**

I. Introduction

MICROWAVE and millimeter wave frequencies have very important applications in modern society [1]. In particular, the Ka-band frequency range (26.5–40 GHz) is useful for communications, radar, spectroscopy etc. [2]. In these applications, it is very desirable to get an amplifier with high power, high gain, and wide bandwidth.

One of the important features of travelling-wave tubes (TWTs) is operation over a wide bandwidth with high gain. As a consequence, there has been strong interest in developing Ka-band and higher frequency TWTs in the recent years. A slow wave structure (SWS) is a very important part in TWTs. At Ka-band and higher frequencies, the physical dimensions of the various parts of TWTs become quite small [3], providing motivation to adopt microfabrication techniques.

The circular helix is the most commonly used SWS in TWTs. The microfabrication of the circular helix SWS has been reported in [4]-[5] and that of a planar helix has been reported in [6]. While these attempts have been quite successful, the steps involved in microfabrication of helix SWSs are complicated. On the other hand, the meander line structure shown in Fig. 1 has been an attractive SWS due to its simple fabrication, ability to accommodate a sheet electron beam, and a low operating beam-voltage.

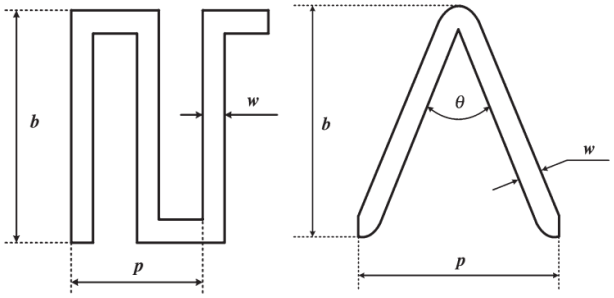

(a) (b)

Fig.1. Two typical meander line SWSs: (a) U shaped and (b) V shaped [9].

There are several shapes of the meander line SWS which have been proposed in the recent past, such as U-shape raised meander line [7], folded meander line [8], V-shaped meander-line [9]-[10]. Although there have been many studies of meander line SWSs, very few fabrication efforts have been reported so far. One such effort was reported in detail in [7] where the meander line SWS was fabricated on a raised dielectric ridge to reduce attenuation and to increase coupling impedance. Multiple W-band SWSs were fabricated on a 4" Si wafer but the microfabrication steps were quite challenging. Moreover, the individual SWS had to be diced and put in a precision-fabricated metal waveguide enclosure for measurements.

In this work, our goal is to design a V-shaped microstrip meander line SWS that operates at Ka-band and is suitable for microfabrication. An important design goal is to be able to carry out on-wafer cold-test measurements since these permit speedy assessment of multiple SWSs. Such a structure was briefly reported in [11]; details of design, fabrication and measurement results are presented here. Of course, once the cold-test phase is completed, normally individual SWSs have to be fitted in a metal enclosure that can be assembled with other parts of a TWT and can be evacuated. In addition, the target is to use the SWS at beam voltages less than 4 kV.

The paper is organized as follows. Section II describes the configuration of the Ka-band V-shaped meander line SWS and

Manuscript received October, 2017. This work was partially supported by a grant from the Office of Space Technology and Industry (OSTIn), Singapore and partially by the Natural Science Foundation of China under Grant 11405137.

S. Wang, S. Aditya and Z. Ali are with the School of Electrical and Electronic Engineering, Nanyang Technological University, Singapore 639798 (e-mail: wangsm@ntu.edu.sg; sheel.aditya@ieee.org). S. Wang is also with the School of Physical Science and Technology, Southwest Jiaotong University, Chengdu 610031, China. J. Miao and X. Xia are with the School of Mechanical and Aerospace Engineering, Nanyang Technological University, Singapore.

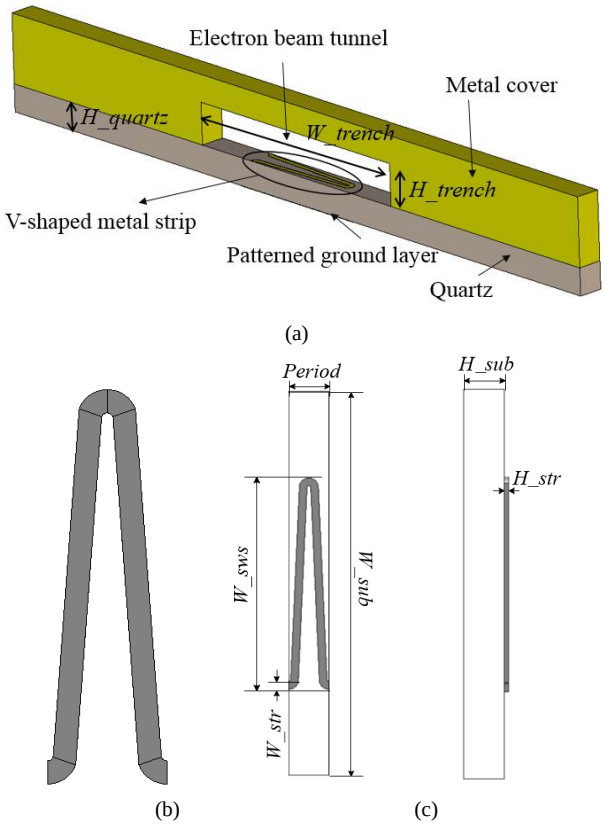

Fig. 2. (a) 3D model (b) front view and (c) side view and dimensional parameters of the modified V-shaped meander line SWS.

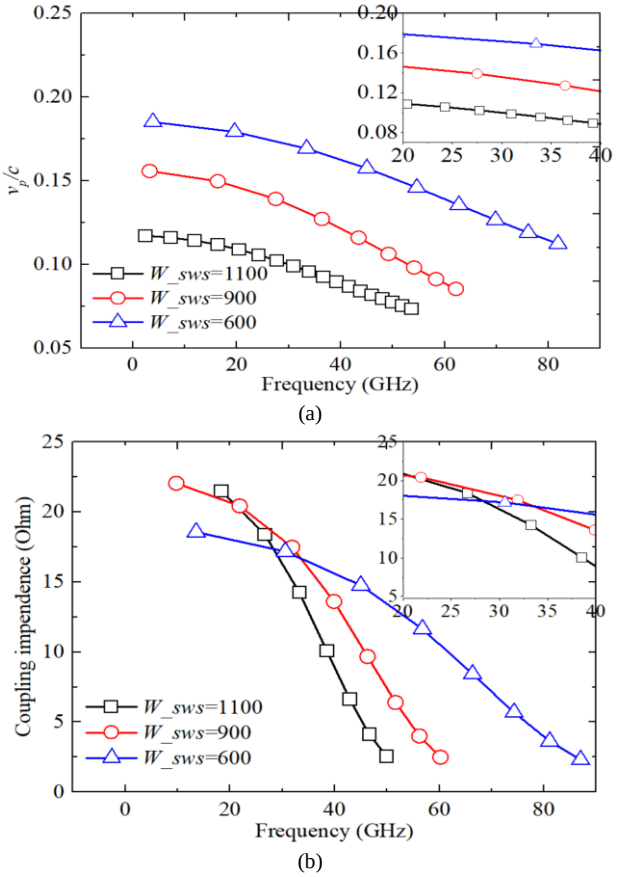

Fig. 3 (a) Dispersion and (b) coupling impedance characteristics of the Ka-band V-shaped meander line SWS with different widths *W_sws* (in μm). Inset figures show the results for the 20-40 GHz frequency range.

its dispersion and coupling impedance. Section III presents the design of the CPW feed and electrical shield for the meander line SWS. Section IV describes the microfabrication and assembly. Section V presents the on-wafer cold-test measurement results and discussion on the results. In section VI, beam wave interaction for the V-shaped meander line SWS is studied by using PIC simulation. Section VII summarizes the paper.

II. Ka-band V-shaped Meander Line SWS

To simplify the fabrication and to realize on-wafer measurements, the basic V-shaped meander line shown in Fig. 1(b) has been modified as shown in Figs. 2(a) and (b). As shown in Fig. 2 (b), the sharp inner bends are replaced by a circular arc which is easier to achieve faithfully in photolithography. Secondly, to avoid dicing to extract individual SWSs and using a metal enclosure for testing, patterned ground plane on the backside as well as an inverted U-shaped metal cover on top are included to provide electrical shielding. Thirdly, the input/output of the meander line SWS transition to 50-ohm coplanar waveguide (CPW) pads for on-wafer measurement on a probe-station. With such a configuration, all the SWSs fabricated on a wafer can be measured in a single setup.

Boron Nitride (BN) is a popular substrate material in the design of microstrip meander line SWS due to its relatively low dielectric constant (4), low loss tangent (3×10^{-4}), and good thermal conductivity (30 W/K/m). Quartz is a competitive material with BN since it also has a relatively low dielectric constant of 4.43 and has a very low loss tangent of 3×10^{-5} at 30 GHz. Although the thermal conductivity of quartz at 1.4 W/K/m is modest, as shown in [12] heat dissipation can be very good when the SWS is in intimate contact with the quartz substrate. Especially, the cost of quartz is much lower and the microfabrication based on quartz wafers is well-developed. Thus quartz is selected as the substrate instead of BN.

As shown in Fig. 2, the proposed configuration of the V-shaped meander line SWS consists of a quartz substrate supporting the V-shaped meander-line pattern on the top surface. The electron beam flows inside the metal cover, in proximity of the meander-line pattern. The main dimensions of the SWS are labelled in Fig. 2. The width and height of the trench (electron beam tunnel) in metal cover are *W_trench* and *H_trench*, respectively; *W_str* and *H_str* are respectively the strip-width and thickness of the microstrip, and *W_sws* and *W_sub* are the widths of the SWS and substrate, respectively. *H_sub* is the height of the substrate.

The characteristics of the proposed SWS have been studied by using Eigenmode solver of CST Microwave Studio [13]. It is known that a relatively flat dispersion curve can be obtained by changing the meander line dimensions. But in this work the dimensions are dictated more by the fabrication accuracy achievable in our research group, and to make the corresponding TWT operate with a beam voltage less than 4

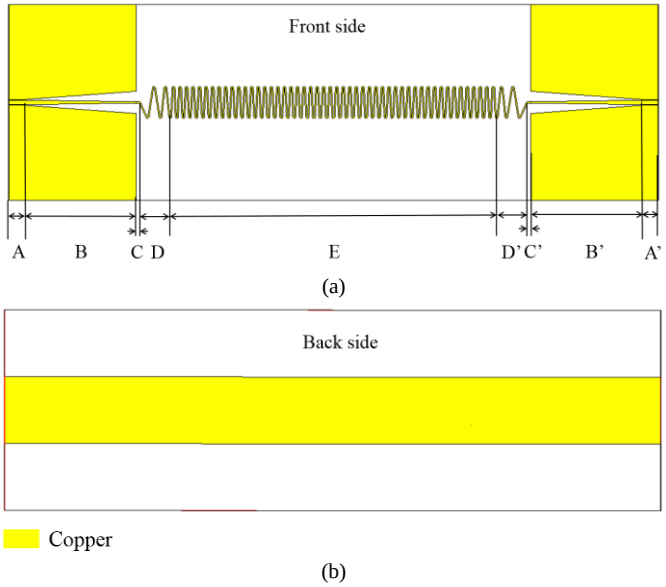

Fig. 4 V-shaped meander line SWS together with CPW to microstrip transitions: (a) Front side and (b) back side.

kV, which is the maximum voltage of the power supply in our group.

Fig. 3 (a) shows the normalized phase velocity of the proposed configuration for different widths *W_sws* of the meander line, with the other parameters fixed as follows: *W_trench*=2000 μm, *H_trench*=300 μm, *W_strip*=40 μm, *W_sub*=6000 μm, *H_sub*=200 μm, and *H_str* =2 μm. It can be seen that the phase velocity depends on the width of the meander line. When *W_sws* is 1100 μm, the normalized phase velocity is 0.1 at 30 GHz and the corresponding operating voltage is ~3.5 kV.

Fig. 3 (b) shows the coupling impedance at the center of the electron beam tunnel which is at a height of 150 μm above the meander-line. Apart from the phase velocity, the width of the SWS also has an effect on the electric field strength; both of these effects impact the coupling impedance. The coupling impedance is about 14 Ohms at 30 GHz for *W_sws* = 1100 μm.

III. CPW Feed and Elctrical Shielding

On-wafer measurements using CPW probes can provide cold-test parameters of the SWS very conveniently. For this purpose, tapered CPW sections are added to achieve impedance match between the input/output of the SWS and 50-Ohm CPW pads. CST microwave studio is used to check the cold-test S-parameters of the V-shaped meander line SWS together with such microstrip-to-CPW transitions.

Fig. 4 (a) shows the front side of the SWS pattern. As shown, the entire length of the SWS can be divided into nine segments: A and A' are the CPW pads with port impedance of 50 Ohm; B and B' are tapered CPW sections; C and C' are straight microstrip sections, which have the same strip-width as the meander line microstrip; D and D' are tapered periods; E is the main V-shaped meander line SWS. The optimized length of the segments are as follows: *LA*=*LA'*=500 μm, *LB*=*LB*'=3400 μm, *LC*=*LC*'=100 μm, and *LD*=*LD*'=940 μm.

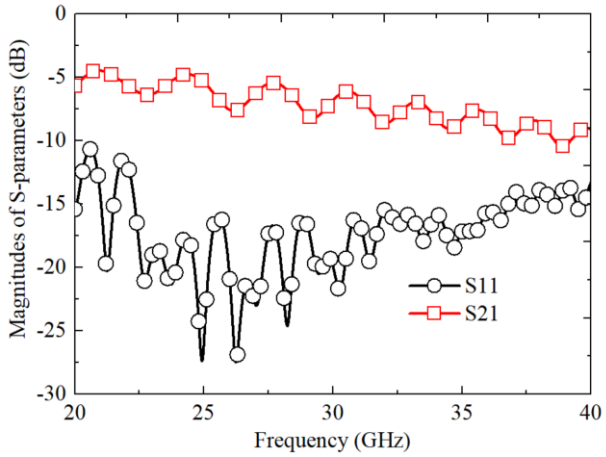

Fig. 5 S-parameters of the V-shaped meander line SWS.

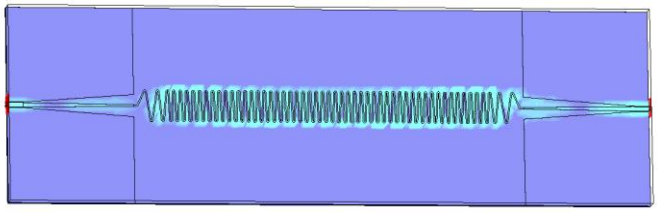

Fig. 6 Absolute electric field on the microstrip V-shaped meander line SWS.

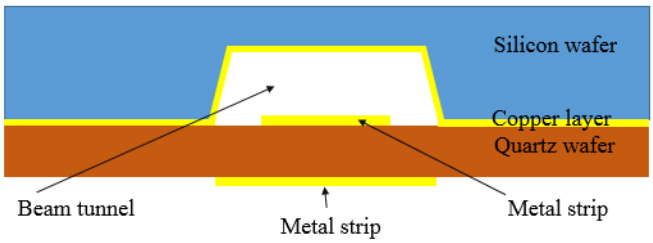

Fig. 7 Fabrication model of the V-shaped meander line SWS.

Since the maximum separation between the probes on the wafer probe station available to us is restricted, the number of periods is kept as 50. The overall length of the SWS including the CPW transitions is about 19.9 mm. Fig. 4(b) shows the pattern on the backside of the quartz substrate. The metal ground plane is truncated to cut off the transverse leakage of the signal. Effective electrical shielding can be realized by adjusting the width of the truncated ground plane. In our design, this width is 3400 μm.

Fig. 5 shows the S-parameters for the third mode of the CPW port. Due to the ground plane below the CPW pads, the first mode of the CPW port is the waveguide mode and the third mode is the typical CPW symmetric electric field mode. The background is set to vacuum and the boundary is set to open (add space). In the 22~36 GHz frequency range, S11 is less than –15 dB and S21 is about – 7 dB at 30 GHz.

Fig. 6 depicts the distribution of the absolute E-field on the SWS, indicating that the electric field does not change significantly along the meander line. Thus it can be claimed that the truncated backside ground metal strip together with the top metal cover can achieve effective electrical shielding.

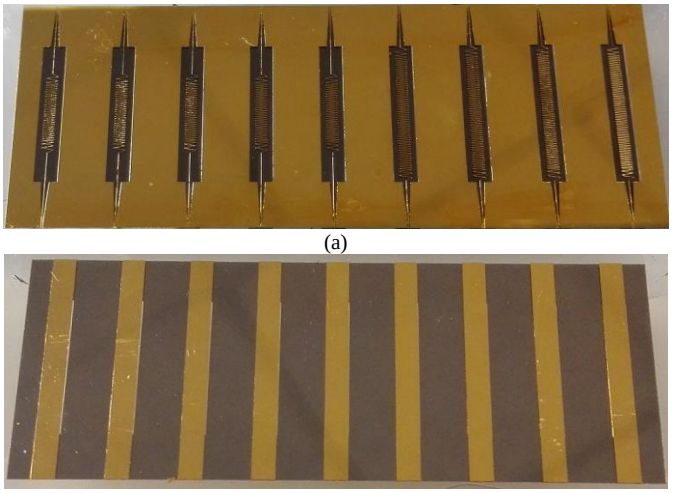

(a)

(b)

Fig. 8 Fabricated V-shaped meander line SWSs on quartz: (a) Front side and (b) back side.

IV. Microfabriction And Assembly

The fabrication model of the SWS is shown in Fig. 7. As mentioned in Section II, the thickness of the metal strip *H_str* has been chosen as 2 μm since this can be easily realized using copper sputtering. Otherwise, electroplating may be required to produce a thicker metal strip, which makes the fabrication complex. We also use a 20 nm thick titanium layer below Cu and a 20 nm thick gold layer over Cu. The meander-line pattern with the CPW transitions on the front surface of quartz wafer and truncated ground plane on the back surface are realized by metal-sputtering followed by photolithography and etching of multiple metal layers.

The top metal cover is realized by using a silicon wafer in which a trench is made using wet-etching and a copper layer is sputtered on the trench-side surface. The two wafers are bonded using a low-loss conductive glue. Alignment marks on both wafers guarantee the accuracy of alignment.

Fig. 8 shows the fabricated microstrip meander line SWSs on quartz wafer. SWSs with two different lengths corresponding to 25 and 50 periods have been fabricated. The separation between the input/output CPW pads is kept the same for all SWSs by including microstrip sections of appropriate length. There are 14 short SWSs and 15 long SWSs on a 4" quartz wafer. The measurements show that the fabricated strip width is 36~38 μm (design value: 40 μm), the CPW signal line width is 136~138 μm (design value: 140 μm), while the CPW gap width is 19~21 μm (design value: 18 μm).

Fig. 9 shows the assembled quartz wafer and silicon cover. The meander line SWSs are covered by the metalized silicon cover while the CPW pads are exposed and accessible for on-wafer measurement.

V. Measurement Results and Discussion

The S-parameters of the fabricated V-shaped meander line SWSs are obtained by on-wafer measurements and compared with simulation results. As marked in Fig. 10, a1 and a2 are results for the 25-period SWSs while b1 and b2 are results for the 50-period SWSs. Simulated a and simulated b are the

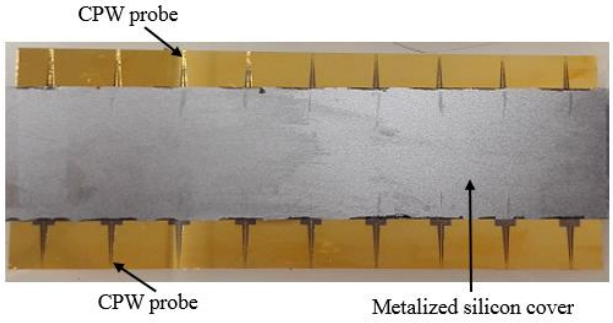

Fig. 9 Assembly of the quartz wafer and silicon cover.

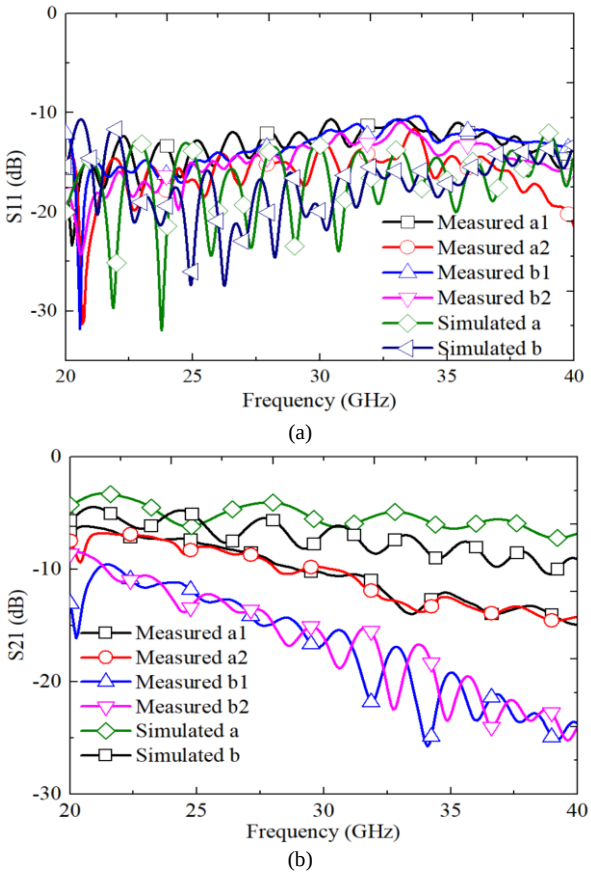

Fig. 10 Comparison of S-parameters between experiment and simulation. (a) S11, and (b) S21.

simulated results for the 25-period and 50-period structures, respectively.

Figure 10 (a) shows that all the measured structures have very similar S11 and it is better than −10 dB in the frequency range of 20-40 GHz. The simulation results for the short and long structures are better than −14 dB and −15 dB, respectively, in the frequency range of 25-36 GHz.

Fig. 10 (b) shows the measured and simulated S21. In general, the curves show that S21 gets worse as frequency increases. For structures with the same number of periods, measured S21 are quite similar. The average difference between the simulated S21 for the short and long structures is about 2.0 dB, which should be the theoretical insertion loss for the 25-period V-shaped meander line. On the other hand, the

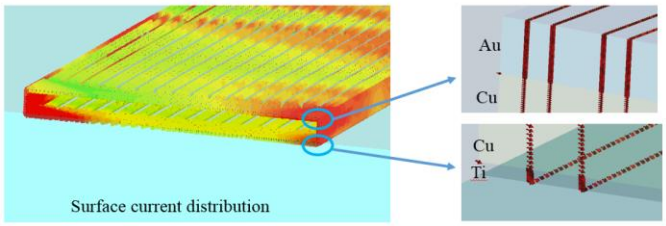

Fig. 11 The surface current distribution on the three-layer microstrip.

average difference between the measured S21 values is about 5.5 dB. It is clear that the measured insertion loss is much higher than the simulated loss.

After a detailed study, the reason for the higher loss is attributed to the conductor loss of the meander line strip. As the tanδ of quartz is very small (3×10^{-5}), the dielectric loss is negligible compared to the conductor loss. The conductor loss is determined by the dimensions and conductivity of the microstrip line. The fabricated meander line consists of three layers: 20 nm titanium, 2 μm copper and 200 nm gold. The overall conductivity of the fabricated microstrip line can be calculated using the formulas listed in [14] and it comes to about 2.9×10^{6} S/m. This value is quite close to that of titanium, which is 2.38×10^{6} S/m. The simulation results assume just a copper layer with conductivity 2.2×10^{7} S/m. Thus it is likely that the extra loss is caused by the titanium layer. Therefore we carry out further simulations as described next.

A three-layer microstrip (20 nm titanium, 2 μm copper and 20 nm gold) on quartz is simulated using CST Microwave Studio. The conductivities are set to 2.4×10^{6} S/m, 2.2×10^{7} S/m and 4.5×10^{7} S/m, respectively. Fig. 11 shows the surface current distribution on the three-layer conductor. There are surface currents on three surfaces of Ti (bottom and two sides) and gold layers (top and two sides), and two side surfaces of copper layer. Due to the skin effect, there are stronger surface currents on the gold and titanium layers than on the copper layer. Consequently, the loss for the titanium layer is about three times higher than that for the copper and gold layers.

Further simulation results show that the insertion loss of such a three-layer microstrip is about 0.086 dB/mm. The physical length of the 25-period V-shaped meander line is about 55 mm, leading to an estimated loss of 4.73 dB. The effect of surface roughness increases the loss further. Thus the measured loss value can be considered to match the estimate well. To further support this conclusion, Fig. 12 shows the simulated S21 for a single conducting layer with conductivity 2.38×10^{6} S/m together with the measurement results for the 50-period SWS. The results match very well up to 28 GHz; beyond that, the average values of the two results differ by 1-2 dB only.

In view of the above discussion, one solution to reduce the insertion loss is to avoid use of low conductivity titanium layer. Our simulation and measured results indicate that using just aluminum for the meander line SWS can give a lower resistance and insertion loss. A sputtered 2 μm layer of aluminum on quartz shows a good adhesion too. More advanced techniques such as selective laser sintering of copper [15] together with a thicker copper layer should lead to even lower insertion loss.

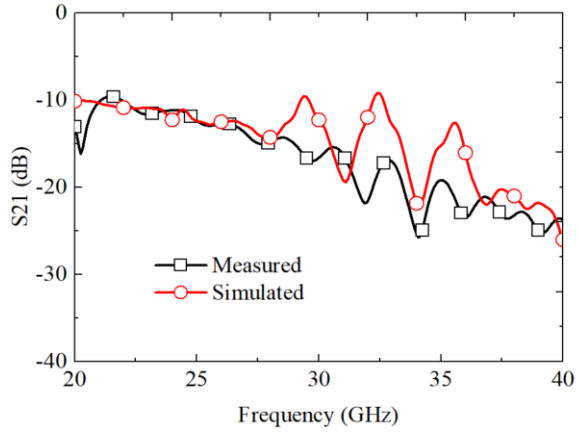

Fig.12 Comparison between simulated (for a conducting layer with conductivity 2.38×10^{6} S/m) and measured S21 of the 50-period microfabricated V shaped meander line SWS.

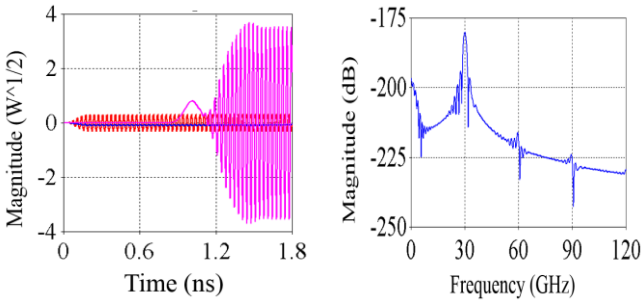

(a) (b)

Fig. 13 PIC simulation results at 30 GHz. (a) Input and output signal; (b) Fourier transform of the output signal.

VI. Beam Wave Interaction

The hot-test parameters of the proposed V-shaped meander line SWS for TWT application are estimated using PIC solver of CST Particle Studio [13] for the structure with discrete ports. The S-parameters of a 50-period SWS are determined by using CST microwave studio first. The results show that S11 is less than −20 dB in the frequency range of 15-40 GHz when the port impedance is 106 Ohm; S21 is about −5 dB at 30 GHz when the metal strip is set to 2 μm copper with a conductivity of 2×10^{7} S/m. This is the insertion loss value that can be expected by using single layer aluminum or copper metallization mentioned in the previous section. The number of periods used in PIC simulation is 170. An e-beam with beam voltage of 3.6 kV and current of 50 mA is applied centrally in the electron-beam tunnel. The rectangular cross section of the e-beam has an optimized width of 700 μm and a thickness of 150 μm. A uniform focusing magnetic field of 0.4 T is used.

Fig. 13 (a) shows the input and output signals with magnitudes 0.32 and 3.54, respectively. The corresponding peak output power is 12.53 W for an input peak power of 0.1 W, indicating a gain of 21 dB. Fig. 13 (b) presents the spectrum of the output signal, showing a clean signal at 30 GHz.

The output power vs. frequency curve is shown in Fig. 14. The maximum output power is 14.5 W at 34 GHz, with a gain of 21.6 dB. In the frequency range of 28-36 GHz, the output power is higher than 7.1 W and gain drop is less than 3 dB, showing a 3 dB bandwidth of about 25% centered at 32 GHz.

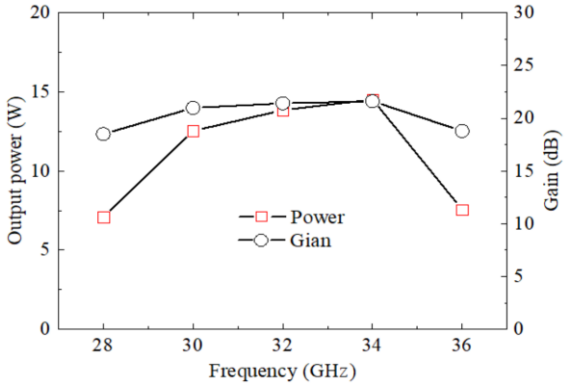

Fig. 14 Output power and gain at different frequencies of the microstrip V shaped meander line SWS.

VII. Conclusion

This paper has described the design, simulation, microfabrication and measured on-wafer cold-test results of a V-shaped microstrip meander line SWS operating at Ka-band frequencies. The SWS design incorporates CPW pads as well as electrical shielding to enable on-wafer cold-test measurements. The SWS has been fabricated on a 4" quartz wafer using Ti/Cu/Au metallization. A 4" silicon wafer with a metallized trench has been used to provide shielding. On-wafer measurements indicate a rather high insertion loss of ~5 dB for a 25-period SWS. The main reason for the high loss is determined to be the presence of the thin Ti layer between the Cu layer and quartz substrate. It is shown that the use of thicker single layer aluminum or copper can bring down the insertion loss. PIC simulation results have been presented; for a sheet electron beam with voltage and current of 3.6 kV and 50 mA, respectively, the output power can potentially reach 14.5 W at 34 GHz with a gain of 21.6 dB with the 3 dB bandwidth of about 25% centered at 32 GHz.

References

[1] R. J. Barker, N. C. Luhmann, J. H. Booske, and G. S. Nusinovich, 'Modern microwave and millimeter-wave power electronics', *IEEE Press*, USA, 2005.

[2] Csere, Csaba , 'Radar Wars: Upping the Ante', *Car and Driver*. Vol. 38 (4), pp: 153 1992.

[3] A. S. Gilmour, Jr., "Principle of Traveling Wave Tubes," *Artech House*, Inc., 1994.

[4] C. L. Kory, J. A. Dayton, G. T. Mearini, D. Malta, M. Lueck, K. Gilchrist, and B. Vancil, "95 GHz helical TWT design," *Proc. IEEE Int. Vac. Electron. Conf.*, Rome, 28–30 April, 2009, pp: 125-126.

[5] M. R. Lueck, D. M. Malta, K. H. Gilchrist, C. L. Cory, G. T. Mearini, and J. A. Dayton, "Microfabrication of diamond-based slow-wave circuits for mm-wave and THz vacuum electronic sources," *Journal of Micromechanics and Microengineering*, 21 (2011) 065022 (7pp), May 2011.

[6] C. Chua, J. M. Tsai, S. Aditya, M. Tang, S. W. Ho, Z. Shen, and L. Wang , "Microfabrication and characterization of w-band planar helix slow-wave structure with straight-edge connections," *Electron Devices, IEEE Transactions on*, vol. 58(11), pp. 4098-4105, 2011.

[7] S. Sengele, H. Jiang, J. H. Booske, C. L. Kory, D. W. van der Weide, and R. L. Ives, "Microfabrication and characterization of a selectively metallized w-band meander-line TWT circuit" *Electron Devices, IEEE Transactions on*, vol. 56(5), pp: 730-737, May 2009.

[8] M. Sumathy, S. K Datta, and L. Kumar, "Folded meander-line slow-wave structure for millimeter-wave TWTs," *IEEE International Vacuum Electronics Conference*, 2013, Paris, France, pp: 1-2, Aug. 2013.

[9] F. Shen, Y. Wei, H. Yin, Y. Gong, Xiong Xu, S. Wang, W. Wang and J. Feng, "A Novel v-shaped microstrip meander-line slow-wave structure for W-band MMPM," *Plasma Science, IEEE trans. on*, Vol. 40(2), pp: 463 – 469, Feb. 2012.

[10] F. Shen, Y. Wei, Xiong Xu, Yang Liu, M. Huang, T. Tang, Z. Duan and Y. Gong, "Symmetric double v shaped microstrip meander-line slow-wave structure for W-band traveling-wave tube," *Electron Devices, IEEE trans. on*, Vol. 59(5), pp. 1551 – 1557, May 2012.

[11] S. Wang, S. Aditya, "A microfabricated v-shaped microstrip meander-line slow-wave structure", *IEEE International Vacuum Electronics Conference*, 2017, London, UK, pp: 1-2, Apr. 2017.

[12] C. Zhao, S. Aditya, S. Wang, J. Miao and X. Xia, "A wideband microfabricated ka-band planar helix slow-wave structure," *Electron Devices, IEEE trans. on*, Vol. 63(7), pp. 2900 – 2906, July 2016.

[13] *Introduction of CST Microwave Studio*, accessed on 1 Dec. 2016. [Online] https://www.cst.com/products/cstps

[14] I. Bahl and P. Bhartia, "Microwave Solid State Circuit Design (Second Edition)", *WILEY-INTERSCIENCE*, pp: 36-37, 2003.

[15] A. Galdetskiy and E. Rakova, "New slow save structure for W-band TWT", *IEEE International Vacuum Electronics Conference*, 2017, London, UK, pp: 1-2, Apr. 2017.